Enhancement of Particle Collection Efficiency in Electrohydrodynamic Atomization Process for Pharmaceutical Particle Fabrication

ARTICLE *in* INDUSTRIAL & ENGINEERING CHEMISTRY RESEARCH · NOVEMBER 2010

Impact Factor: 2.59 · DOI: 10.1021/ie1009662

3 AUTHORS, INCLUDING:

Amalina Attia
Agency for Science, Technology and Resea…
13 PUBLICATIONS **289** CITATIONS
SEE PROFILE

Chi-Hwa Wang
National University of Singapore
224 PUBLICATIONS **4,647** CITATIONS
SEE PROFILE

Enhancement of Particle Collection Efficiency in Electrohydrodynamic Atomization Process for Pharmaceutical Particle Fabrication

Alireza Rezvanpour, Amalina B. E. Attia, and Chi-Hwa Wang*

Department of Chemical & Biomolecular Engineering, National University of Singapore, 4 Engineering Drive 4, Singapore 117576

In the present work, Electrohydrodynamic Atomization was employed to produce biodegradable polymeric microparticles in a new generation of shuttle glass chamber. The effects of different parameters including solution flow rate, nitrogen flow rate, nozzle, and ring voltage on the particle collection efficiency and residual amount of organic solvent in collected particles were investigated systematically. The Taguchi (a combined experimental and statistical) method was used to obtain the optimal collection conditions for the particle collection efficiency. It was found that the important factors affecting particle collection efficiency were given in the following order—solution flow rate, nitrogen flow rate, ring, and nozzle voltage. It was also found that voltage difference between nozzle and ring can significantly affect the particle collection efficiency. Duration of the process, polymer material, and electrical conductivity of the solution were the other factors that affected particle collection efficiency. It was found that solution flow rate and nozzle voltage can considerably affect the size of fabricated particles. Gas Chromatography/Mass Spectrometry was used to determine the residual content of Dichloromethane (DCM) in the collected particles. For all 16 trials, the residual DCM content of the particles fabricated using the EHDA method was well within the limit of safety standards (600 ppm) at the end of process without engaging any additional freeze-drying process. In summary, high collection efficiency and minimum residual solvent in collected particles can be achieved by adjusting the operating parameters and geometrical characteristics of the system.

Introduction

EHDA is a well-known phenomenon for production of fine droplets of uniform size.[1,2] EHDA in the cone-jet mode has been studied for many years.[3] The main concept here is applying an electric field on pendant and flowing droplets (through a capillary) to atomize them. The droplet profile as a function of applied voltage can be studied as the main data extracted from EHDA experiments. Some research results show that if the potential is lower than that required for liquid instability, electrostatic atomization is not possible. In addition, the conductivity and flow rate of the liquids play a major role in the electrostatic disruption of liquids flowing through the capillary.[4] Physical properties of liquid like viscosity and electrical conductivity are the other important factors that have a significant effect on the formation of Taylor cone at the tip of the capillary in EHDA process.[5] The stability and atomization characteristics of electrohydrodynamic jets can be experimentally investigated.[6–8] According to some research results, the cone-jet mode exists at lower levels of applied voltage, while the multijet mode exists at higher voltage levels.[9,10] Stable operation in the cone-jet mode produces droplets that are roughly 3 orders of magnitude smaller than the capillary diameter.[11,12] One of the most important applications of EHDA process is production of controlled size and controlled physical property polymer particles. The research results demonstrate that water-soluble and water-insoluble, low dispersity polymer particles can be readily prepared by the EHDA process with geometric mean diameters in the micrometer size. It shows that this method can be used for the production of advanced polymer materials.[13] Therefore, EHDA can be used in fabrication of biodegradable polymeric micro- and nanoparticles which are widely used in drug delivery systems.[14,15] The practical aspects of production of polymeric particles loaded with a drug by the electrohydrodynamic atomization method are presented in some research articles. The research results state that quickly evaporating solvents have a tendency to form hollow particles. Drug release rate from hollow particles is substantially higher than from solid ones.[16] The electrospray process in the dripping mode can be used for cell microencapsulation. Microencapsulation of living cells with controllable size and narrow size distribution can be obtained using electrospray in a dripping mode and can be stabilized by a ring electrode. The findings of this process are very useful in the scaling up of the aforementioned process to generate large quantities of microbeads. These microbeads can be employed as biosorbents for removal of metal ions in water and as delivery devices for controlled release of drugs. Moreover, the effect of operating conditions like electrical field strength and liquid and inert gas flow rate on particle size and morphology are studied and the results are reported in some research articles.[17–20]

Particle collection efficiency and residual solvent in collected particles are two important issues in particle fabrication using the EHDA process that are not addressed in the literature. These two factors are exceedingly important for designing an EHDA system especially from the point of view of operating costs. Since the materials used for pharmaceutical particle fabrication are expensive, higher particle collection efficiency is extremely desirable. Moreover, an allowable concentration of residual solvent in collected particles after the EHDA process and before freeze-drying is desirable because it eliminates freeze-drying as an additional energy-consuming process. The present work aims to employ EHDA technology to fabricate particles in a new generation of shuttle chamber. Here, we investigated the production process with a focus on the particle collection efficiency and residual solvent in the collected particles. The experiments are designed based on the Taguchi (combined statistical and experimental) optimization method. Subsequently,

* To whom correspondence should be addressed. Tel: 65-6516-5079. Fax: 65-6779-1936. E-mail: chewch@nus.edu.sg.

10.1021/ie1009662
Published on Web 11/16/2010

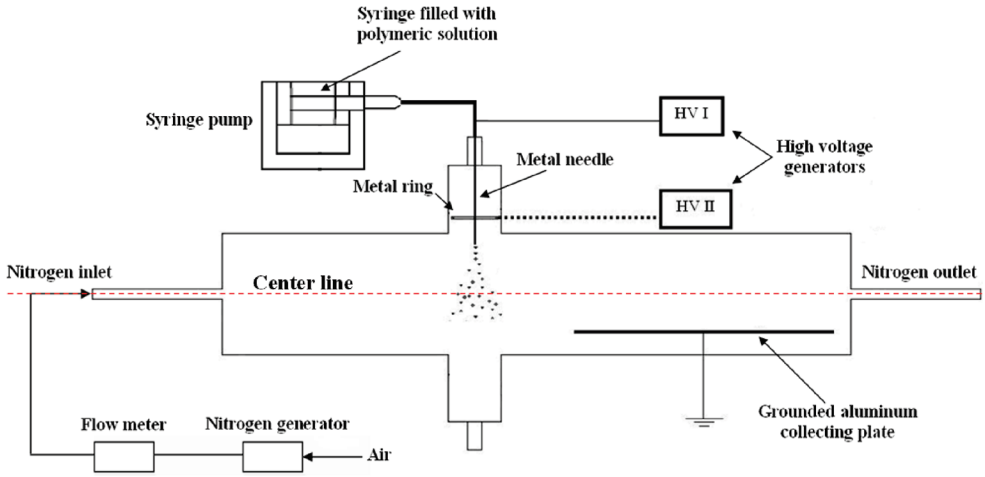

Figure 1. Apparatus used in the experiments.

the results are summarized in different tables and figures. In the present work, we aim to develop a deeper understanding of the EHDA process for polymeric particle fabrication and also to achieve better collection efficiency and solvent evaporation by adjusting some of the operational and geometrical parameters.

Materials and Methods

EHDA Setup. In the experimental apparatus used in this study (shown in Figure 1), a shuttle glass chamber was used to enclose a nozzle (0.41 mm ID) and a ring (40 mm ID) electrode, which were both applied with high electrical potential relative to the ground plate, together with a grounded collecting plate. Since a sharp tip may result in an unstable Taylor cone, the nozzle tip was flattened on sandpaper to give a flat and blunt tip. There are two advantages for using the shuttle glass chamber in this study. First, this shuttle chamber provides an isolated environment for the control of the ambient condition and collection of the particles by preventing unwanted external contaminations. Second, a cross-flow of inert gas is used inside the chamber to aid both the evaporation of the organic solvent from the droplets and the collection of the particles using a pneumatic conveying method. The chamber used in this experiment is modified from the one used by Ding et al., Xie et al., and Yao et al. Three major improvements could be identified in the new type of the chamber upon comparison with the previous prototypes. First, the new chamber is completely cylindrical, whereas the previous chambers had two conical ends. Second, the particles fabricated in the new shuttle chamber are collected inside the vessel and far away from the spray zone. Finally, nitrogen inlet and outlet in the new vessel had larger diameters than previous types. These modifications markedly affected the inert gas reverse flow and flight time of the particles inside the chamber. Lesser reverse flow, higher particle collection efficiency, and lower amount of residual organic solvent in the collected particles were the main advantages of the above-mentioned modifications.

The spray encapsulation section includes the nozzle-ring configuration and the surrounding chamber. The nozzle and the ring were connected to two high-voltage DC power supplies independently (Glassman High Voltage Inc., NJ, USA), forming the electric field for EHDA. A high positive electrical potential relative to ground was applied to the nozzle while a lower positive electrical potential was applied to the ring. The ring was deployed to render better control of the EHDA spray, while the ground plate acted as the counter electrode to the nozzle and ring for discharging the collected particles. In this study four different voltages are applied to both nozzle and ring. These applied voltage difference values are listed in Table 1.[18–23] The ground plate is also the collecting location of the particles formed. The distance between the nozzle tip and the collecting plate is 20 cm which is larger than the distance mentioned in the previous works reported by Ding et al., Xie et al. and Yao et al.[20,40,41] This large distance may give the droplets more flying time and thus resulting in evaporating more organic solvent. Solution was pumped out using a programmable syringe pump (Stoeting Co., Illinois, USA). Nitrogen as inert gas was connected to the left end of the chamber and the other end was also open as nitrogen outlet such that the collection rate of the particles could be adjusted through a pneumatic conveying method. "Pneumatic conveying" or "pneumatic transport" refers to the use of a gas to transport a particulate solid through a pipeline or vessel.[24] In this process, nitrogen is used as the conveying gas for flying the particles toward the collecting plate. Details of the nitrogen and solution flow rates are listed in Table 1. In contrast, relevant experimental conditions and setup characteristics are listed in Table 2.

Table 1. Controllable Factors and Their Levels Used in the Experiments

	factors	level 1	level 2	level 3	level 4
1	nozzle voltage (kV)[a]	9.0	8.5	8.0	7.5
2	ring voltage (kV)[a]	7.0	6.5	6.0	5.5
3	soln. flow rate (mL/h)	2.5	2.0	1.5	1.0
4	nitrogen flow rate (L/min)	35	30	25	20

[a] Values shown are relative to the ground.

Materials. Poly (D,L-lactide-co-glycolic acid) (PLGA) with an L:G molar ratio of 85:15 and poly lactic acid (PLA) were purchased from Sigma Aldrich (St. Louis, MO USA). Paclitaxel and organic salt, Tetra-butyl Ammonium Tetra-Phenyl Borate (TATPB), were purchased from Bristol-Myers Squibb (UK). Dichloromethane (DCM) and *N*,*N*-dimethylformamide (DMF) were purchased from Tedia Company (Fairfield, OH, USA). Conductivity meter (Model 3200, YSI incorporated, OH, USA) was used to measure the electrical conductivity of DCM. The electrospray solution would contain PLGA at 8% w/v of DCM and Paclitaxel at 20% w/w of PLGA. An Ultrasonicator (Cole-Parmer Instrument Co., Illinois, USA) was used to dissolve the components of the mixture homogeneously for about 15 min. The physical properties are listed in Table 2.

Table 2. Experimental Conditions, Setup Characteristics and Physical Properties of the Used Materials

inner diameter of the nozzle	0.41 mm (27 Gauge)
diameter of the ring	33 mm
thickness of the ring	3 mm
inner diameter of the chamber	100 mm
length of the chamber	800 mm
diameter of the chamber outlet and inlet	15 mm
collecting plate material	aluminum
collecting plate dimensions	90 mm × 100 mm
distance between nozzle tip and collecting plate	200 mm
distance between collecting plate and center line	35 mm
DCM density	1326.6 kg/m^3
DCM electrical conductivity	0.0025 μS/cm
DCM viscosity	4.4 × 10^{-4} kg/m·s (20 °C)
DCM dielectric constant	9.1 (20 °C)
DMF density	944 kg/m^3
PLGA density	936.71 kg/m^3
PLGA + DCM (w/v = 8%) density	1276 kg/m^3
PLGA + DCM (w/v = 8%) viscosity	8.3 × 10^{-4} kg/m.s
PLA density	1269 kg/m^3
PLGA + DCM (w/v = 8%) density	1283 kg/m^3
PLGA + DCM (w/v = 8%) viscosity	9.1 × 10^{-4} kg/m.s
vacuum permittivity	8.85 × 10^{-12} C^2·s^2/kg.m^3

Quantification of Residual Solvent Content in Collected Particles. The residual solvent content in the fabricated particles is one of the potential concerns for pharmaceutical applications. Since this has rarely been demonstrated by earlier publications, this has been identified as one key feature of investigation in the present study. Standard solutions were prepared with the level of DCM concentrations in DMF ranging from 0.5 to 10 × 10^{-6} ml DCM per ml DMF and stored in the refrigerator before analysis to prevent evaporation of DCM in the mixture.[25]

Gas chromatography/mass spectrometry (GC/MS) was used to determine the residual content of DCM in the fabricated particles. A peak area for DCM which can be defined as "absorbance × time" was obtained for each standard concentration and particles samples. By examining the GC spectra for the standards, a calibration curve can be obtained. The calibration curve is constructed when the integration areas under DCM peaks versus concentrations of DCM in DMF is plotted. The integration areas for each sample were compared with a calibration curve and the corresponding DCM concentrations could be calculated. After identifying the GC spectrum peak as DCM, the area under the peak was integrated and the result is given by the GC/MS computer program. A linear calibration curve was used to relate the integration area and concentration of DCM in DMF.

Experimental Design. A statistical experimental optimization method (Taguchi) is used to determine the optimal collection conditions and to find the main parameters affecting the particle collection efficiency and size of the fabricated particles.[26] The Taguchi method is a useful method for systematic study of different effective factors and it has been applied for many years.[27] The advantages, like prediction of the results with less numbers of experiments and determination of the optimum conditions based upon the obtained results, has made the method very popular in industry as well as in science.[28]

In this work, four different variables were chosen as controllable factors and particle collection efficiency and particle size as the response factors. The choice of the factors was based on a literature survey.[16–19] The choice of the levels was based on prior testing of EHDA process to achieve a stable cone-jet mode at the tip of the nozzle. All factors and their levels were combined into 16 trials. A summary of the factors and their levels in the proposed experimental plan and the results of the experiments are presented in Table 3.

Table 3. Summary of Factors, Levels, Obtained Results (Collection Efficiency) and *S/N* Ratio in Each Trial

trial no.	nozzle voltage (kV)	ring voltage (kV)	soln. flow rate (mL/h)	nitrogen flow rate (L/min)	collection efficiency 1 (%)	collection efficiency 2 (%)	*S/N*
1	9	7	2.5	35	73.5	78.1	37.6
2	9	6.5	2	30	56.1	77.5	36.2
3	9	6	1.5	25	55.1	61.3	35.2
4	9	5.5	1	20	66	81.4	37.2
5	8.5	7	2	25	48.2	52.6	34.0
6	8.5	6.5	2.5	20	75.7	80.1	37.8
7	8.5	6	1	35	79.4	77.7	37.9
8	8.5	5.5	1.5	30	67.5	78.6	37.2
9	8	7	1.5	20	58.2	68.8	36.0
10	8	6.5	1	25	78.9	70.2	37.4
11	8	6	2.5	30	73.1	66.3	36.8
12	8	5.5	2	35	60.5	71.0	36.3
13	7.5	7	1	30	73.1	61.2	36.4
14	7.5	6.5	1.5	35	61.6	68.1	36.2
15	7.5	6	2	20	69.6	54.7	36.7
16	7.5	5.5	2.5	25	62.3	72	36.5

In different set of experiments, two different high molecular weight polymers, PLA and PLGA, were used to prepare the electrospray solution. The aim was to investigate the effect of physical properties of polymer on collection efficiency, shape and size of the fabricated particles.

The electrical conductivity of the organic solvent tends to be low; therefore, electrolytes such as organic salts are commonly used to increase the electrical conductivity of the sprayed solution. The high viscosity of the sprayed liquid combined with low electrical conductivity prevented stable cone-jet mode and production of monodisperse droplets, thus affecting the collection efficiency. For this set of experiments, PLGA or PLA with Paclitaxel (20% w/w) and different amounts of TATPB was dissolved in DCM (8%, w/v) by sonication.

Collection Efficiency Calculation. Collection efficiency (CE) is defined as follows:

$$\text{CE, \%} = \frac{\text{mass of the collected particles}}{\text{total mass of the initial PLGA and Paclitaxel}} \times 100\% \quad (1)$$

Arithmetic Mean Diameter (AD). Scanning electron microscopy (SEM) photos were used to obtain the particle size distribution for each trial. Arithmetic mean diameter was also used to calculate the mean diameter for each trial. Arithmetic mean diameter is defined as follows:[29]

$$\text{AD} = \frac{\sum_{i=1}^{n} d}{n} \quad (2)$$

Force Balance on Falling Particle. Force balance on a falling particle is presented in eq 3.

$$m_p \frac{d\mathbf{u}}{dt} = \sum \mathbf{F} = \mathbf{F}_D + \mathbf{F}_g + \mathbf{F}_B + \mathbf{F}_E + \mathbf{F}_q \quad (3)$$

The magnitude of the drag force[30–33] can be calculated by eq 4.

$$F_D = \frac{1}{2} C_D (\pi R_p^2) \rho_f u_v^2 \quad (4)$$

For Reynolds number larger than 0.4 and smaller than 500, the drag coefficient may be calculated using the following equation.

$$C_D = \frac{24}{Re_p}(1 + 0.15Re_p^{0.687}) \quad (5)$$

Gravitational and buoyancy forces can be incorporated into each other and calculated by eq 6.

$$\mathbf{F}_g + \mathbf{F}_B = \frac{4}{3}\pi R_p^3(\rho_p - \rho_f)g \quad (6)$$

The magnitude of electrical field force can be calculated by eq 7.

$$\mathbf{F}_E = q\mathbf{E} \quad (7)$$

The magnitude of the columbic repulsive force can be calculated by eq 8.

$$\mathbf{F}_q = \sum_{i=2}^{n} \frac{q^{\bullet}q_i}{4\pi\varepsilon_0}\frac{1}{r_i^2}\mathbf{r}_i \quad (8)$$

Results and Discussion

Optimization of Experimental Trials. A parameter which is defined for comparing the trials and the influence of a factor in the Taguchi method is the ratio of the desired factor to the noise created during the experiment, *S*/*N*. This ratio was used for comparing the trials and the influence of a factor in the Taguchi method.[34] Since a higher collection efficiency is desirable in this experiment, "the bigger the better" criterion was chosen for the *S*/*N* ratio. In general, a smaller noise is desirable so a larger *S*/*N* ratio yields results that fulfill the objectives.[35] The following equations show how this ratio can be calculated for an example data set:[35]

$$\mathrm{MSD} = \frac{\sum_{i=1}^{N}\left(\frac{1}{Y_i}\right)^2}{N} \quad (9)$$

$$S/N = -10\log_{10}(\mathrm{MSD}) \quad (10)$$

where MSD is the mean squared deviation from the target value of the response (which is 100% for collection efficiency). Y_1 and Y_2 are the first and second response factors (Collection efficiency 1 and Collection efficiency 2 for each trial in Table 3), and N is the number of observations (here each trial was repeated in duplicate). Since the value of S/N is anticipated to be large, the value of MSD should be small.

The average values of *S*/*N* for different trials are presented in Table 3. It may be seen that the largest value of *S*/*N* is for the trial no. 7 where the nozzle voltage is 8.5 kV, the ring voltage is 6 kV, the solution flow rate is 1 mL/h and nitrogen flow rate is 35 L/min.

The *S*/*N* ratio for a factor may be calculated by averaging the *S*/*N* values at different levels. For example, the *S*/*N* for the third factor, solution flow rate at high level, is equal to the average value of *S*/*N* for each trial where solution flow rate is at the first level, i.e., trials 1, 6, 11, and 16. The *S*/*N* for the other levels is calculated similarly. In Table 4, the *S*/*N* for each level of factor and the differences between levels are presented. A negative sign shows that the effect is decreasing and vice versa. In optimum conditions a positive and larger value of *S*/*N* is desired. Therefore, the levels which give the biggest positive *S*/*N* ratio determine the optimum conditions for the considered factor. Comparison among the *S*/*N* values for different factors shows that the most significant variation is observed for solution flow rate while for the rest of the factors the variation is not very clear.

The quantitative analysis of the influences and the relative importance of the controllable factors may be provided via ANOVA (Analysis of Variance). Table 5 shows the results of this analysis for collection efficiency. The last column in this table shows the percent contribution of each factor which is the most important value achieved. It is defined as the portion of total observed variance in the experiment of each significant factor. A greater value means more contribution to the final results. In comparison with other factors, solution flow rate appears to have the largest contribution to the results.

The other important parameter in Table 5 is the *F*-ratio, which is defined as the ratio of variance due to the effect of a factor to the variance due to the inherent error of the system. Therefore, the case of *F*-ratio less than 1 means that the effect of that particular factor is not important relative to the error term. In Table 5, the *F*-ratio for nozzle voltage is less than 1 and thus the effect may be regarded as insignificant and can be neglected. The *F*-ratio may also be used to rank the factors according to their significance. On the basis of these discussions, Table 5 shows that the important factors in the following order as: (i) solution flow rate, (ii) nitrogen flow rate, and (iii) ring voltage.

In Table 5, the row which is marked as error/others refers to the errors which are caused by uncontrollable factors (noise), and is not included in the experimental data and error. In general, this value should be below 50%, otherwise the results would not be reliable.[28] Here, the calculated error is about 36% which is less than the limit. It means that almost all effective factors have been considered and the error of the experiment is not significant.

ANOVA may be used to estimate the process performance at optimum conditions. The results of estimated performance are listed in Table 6. The collection efficiency at these conditions is given by this analysis as 82.04%. Since the optimum conditions are not belonging to any of the trials in Table 3, a confirmation experiment was performed to verify the predicted result. If the average results of the experiments are within the confidence limit, then the prediction is acceptable. The value of the collection efficiency at optimum conditions was measured as 79.4% and it may be seen that it is within the range of the confidence limit.

Effect of Solution Flow Rate. Figure 2 shows the variation of the collection efficiency versus solution flow rate at optimum conditions listed in Table 6. This figure indicates that collection efficiency drastically decreases with increasing solution flow rate from 1 to 1.8 mL/h. However, the collection efficiency increases as the solution flow rate increases from 1.8 to 2.5 mL/h. Figure 2 shows that the collection efficiency varies significantly with a small change in solution flow rate which confirms the high contribution of this factor presented in Table 6. Grace and Marijnissen (1994) reported that at high solution flow rates, the charges on the liquid at the nozzle tip could not be concentrated as there is more liquid per unit time and there is not enough electrical force to overcome the mechanical forces of liquid motion.

In contrast, at low solution flow rates, the electric charges on the drop at the nozzle tip are sufficient for electrical forces to overcome the surface tension force to achieve jet spraying. Therefore, the spraying is more stable and more particles with smaller size[18] are produced on the collecting plate. As the optimum solution flow rate in this study is 1 mL/h (as shown in Table 6), it shows that this flow rate is low enough to produce

Table 4. *S/N* Ratio for Levels of Each Factor and *S/N* Differences between These Levels Where Particle Fabrication Has Been Optimized

	factors	L1[a]	L2	L3	L4	L2−L1	L3−L2	L4−L3
1	nozzle voltage (kV)	36.6	36.7	36.6	36.2	0.1	−0.1	−0.4
2	ring voltage (kV)	36.0	36.9	36.4	36.8	0.9	−0.5	0.4
3	soln. flow rate (mL/h)	37.2	35.5	36.2	37.2	−1.7	0.7	1.0
4	nitrogen flow rate (L/min)	37.0	36.7	35.8	36.7	−0.3	−0.9	0.9

[a] L1: level 1; L2: level 2; L3: level 3; L4: level 4; L2−L1: difference between levels 1 and 2; L3−L2: differences between levels 2 and 3; L4−L3: differences between levels 3 and 4.

Table 5. Results of Analysis of Variance (ANOVA) for Particle Collection Efficiency for Each Factor

	factors	DOF[a]	sum of squares	variance	*F*-ratio	pure sum	percent
1	nozzle voltage	3	0.614	0.213	0.381	0	0
2	ring voltage	3	1.97	0.656	1.35	1.2	6.852
3	solution flow rate	3	8.19	2.73	4.874	6.51	41.563
4	nitrogen flow rate	3	3.181	1.06	2.321	1.9	15.581
5	error/others	3	1.679	0.559			36.004
6	total	15	15.663				100.0

[a] Degree of freedom.

Table 6. Estimated Performance at the Optimum Conditions

	factors	level description	level	contribution
1	nozzle voltage (kV)	8.5	2	0.209
2	ring voltage (kV)	6.5	2	0.428
3	soln. flow rate (mL/h)	1	4	0.710
4	nitrogen flow rate (L/min)	35	1	0.511

stable cone jet. As solution flow rate increases, high surface tension on the Taylor cone can cease the formation of cone jet mode and converts it to a dripping mode.[36] Moreover, the high collection efficiency at low solution flow rates can also be related to the small size of the fabricated particles.[18] Equation 6 indicates that gravitational force has direct relation with size of the particle and, thus, smaller size of the particles results in lower gravitational and buoyancy forces. As such, the importance of these forces decreases with decreasing size of the particle and electrical field force, therefore, is predominant in these conditions. Electrical field force dominance is favorable for achieving high particle collection efficiency. Consequently, decreasing solution flow rate causes the production of smaller particles and results in higher particle collection efficiency. However, when the solution flow rate is increased further from 1.8 to 2.5 mL/h, the formation of a simple jet can actually occur at higher solution flow rates.[37] This phenomenon occurs because at high solution flow rates, the kinetic energy per unit surface of the liquid at the outlet at nozzle tip is greater than the surface tension of the jet; consequently, simple jet occurs.[38] As the solution flow rate increases, the simple jet mode becomes more stable.[37] The simple jet allows the formation of more particles and the production yield is increased and more particles would be produced on the collecting plate.

Effect of Nitrogen Flow Rate. Figure 3(a) shows the variation of the collection efficiency with nitrogen flow rate at optimum conditions listed in Table 6. Furthermore, Figure 3, parts (b) and (c), also shows the same trend for the other conditions. These figures indicate that collection efficiency slowly decreases with increasing nitrogen flow rate from 20 to 26 L/min. However, the collection efficiency increases as the nitrogen flow rate increases from 26 to 35 L/min.

The variation of collection efficiency for each nitrogen flow rate versus the solution flow rate is presented in Figure 4.

The variation range of the collection efficiency versus nitrogen flow rate is smaller than the corresponding solution flow rate presented in Table 6. According to eq 4, an increase in the nitrogen flow rate can indeed increase the corresponding drag force, which is almost parallel to the electrical field force in this system. However, increasing nitrogen flow rate below 26 L/min does not have an observable effect on drag force. In contrast, it results in enhanced turbulence and eddy of nitrogen flow inside the chamber. This turbulence can cause the particles to circulate inside the chamber and increase the chance of particle deposition on the chamber's walls before reaching the

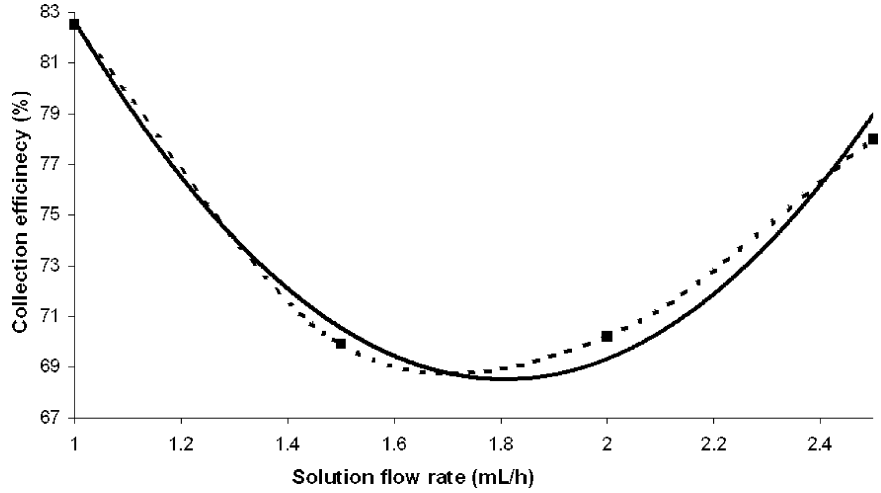

Figure 2. Variation of the collection efficiency versus solution flow rate at optimum conditions. (— Predicted by Taguchi, ---- Experimental results).

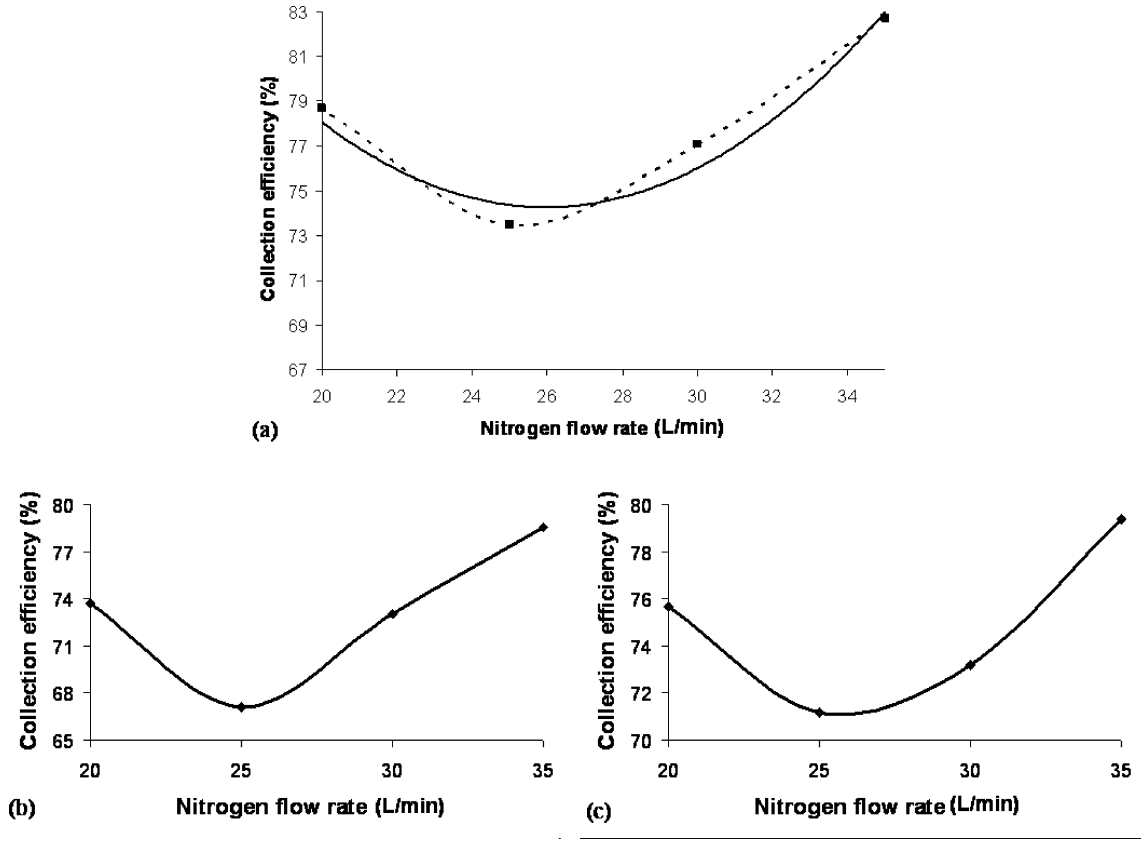

Figure 3. Variation of the collection efficiency versus nitrogen flow rate at (a) optimum conditions shown in Table 6 (— Predicted by Taguchi, ---- Experimental results), (b) Nozzle voltage 8.5 kV, ring voltage 5.5 kV and solution flow rate 1.5 mL/h, and (c) Nozzle voltage 8.5 kV, ring voltage 6.5 kV and solution flow rate 2.5 mL/h.

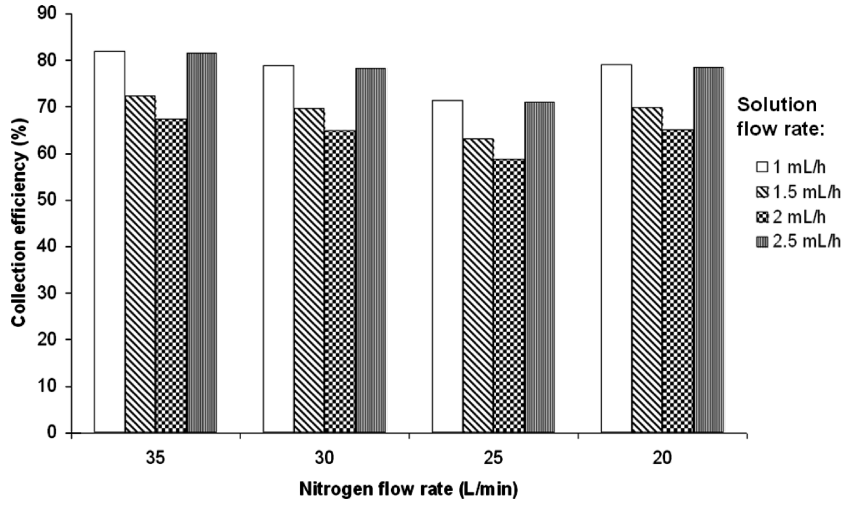

Figure 4. Variation of collection efficiency for four example nitrogen flow rates versus solution flow rate.

collecting plate. Conversely, increasing the nitrogen flow rate from 26 L/min onward has significant effect on enhancing the drag force. In fact, the effect of pneumatic conveying of the particles overcomes the effect of turbulent flow inside the chamber. Furthermore, the cylindrical shape of the glass chamber with an open and wide outlet effectively prevents the reverse flow and circulation of the nitrogen inside the glass chamber. Additionally, the increase in nitrogen flow would also evaporate the solvent on the particles faster and the particles would be less sticky for premature deposition on the chamber's walls. In summary, when nitrogen flow was increased from 20 to 26 L/min, the turbulent flow is probably more significant than the conveying of particles as the nitrogen flow was not strong enough to carry the particles toward the collecting plate. In contrast, the turbulent flow due to the increase nitrogen flow is probably minor as compared to the pneumatic conveying of the particles toward the collecting plate when the nitrogen flow rate is between 26 to 35 L/min.

Effect of Nozzle and Ring Voltages. Figure 5, parts (a) and (b), shows the variation of the collection efficiency versus nozzle and ring voltages respectively at the optimum conditions listed in Table 6. This figure illustrates that collection efficiency increases with increasing nozzle voltage and decreases with increasing ring voltage in a nonmonotonic fashion. The collection efficiency slowly changes with variations in nozzle and ring voltages. Weak effect of these factors on collection

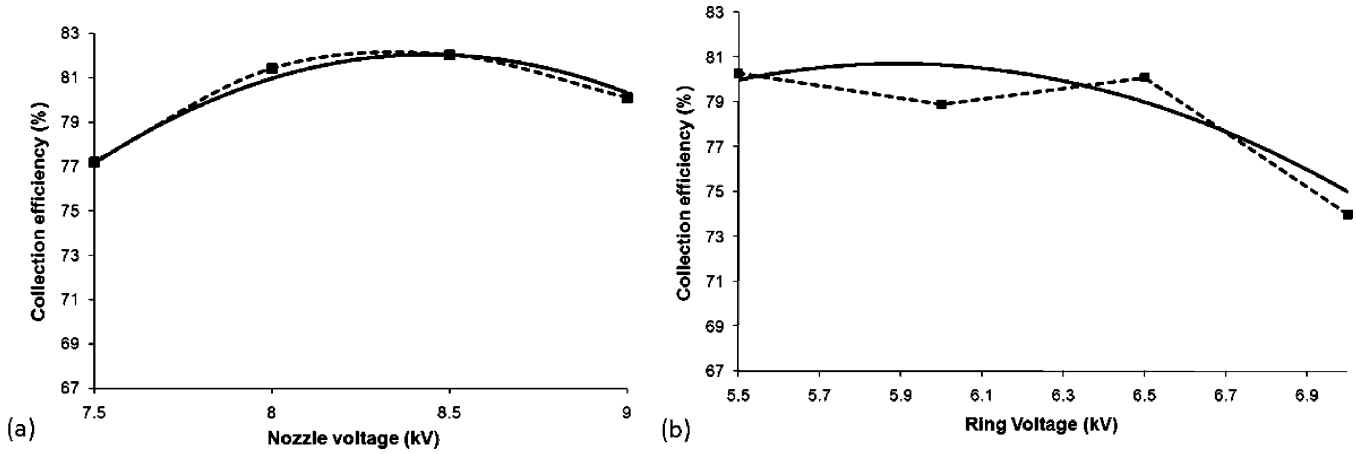

Figure 5. Variation of the collection efficiency versus (a) nozzle and (b) ring voltages respectively at optimum conditions. (— Predicted by Taguchi, ---- Experimental results).

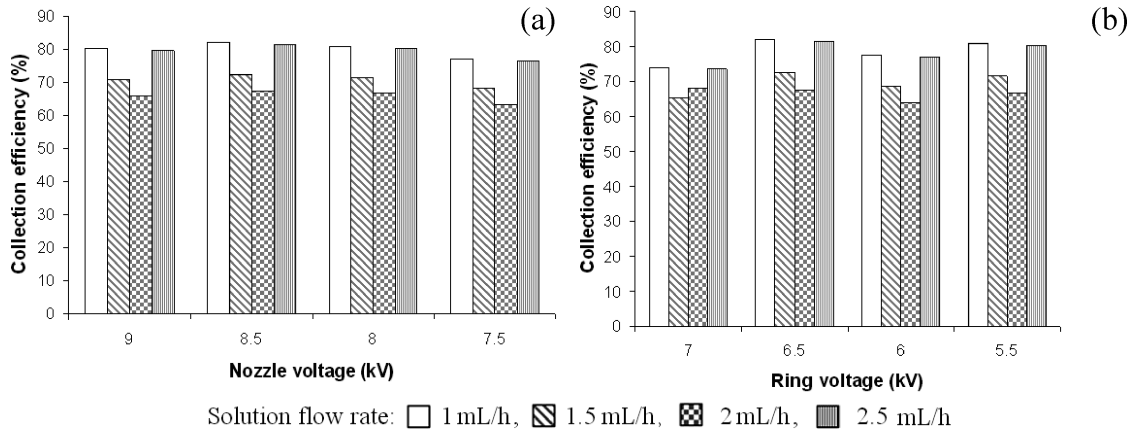

Figure 6. Variation of collection efficiency for each nozzle (a) and ring (b) voltages versus the solution flow rate.

efficiency was previously declared by Taguchi results (Table 6) and can also be verified in Figure 6. The collection efficiency is not strongly influenced by these settings because the combined nozzle and ring system allows the production of a single cone-jet over a wide range of voltage differences. When a single nozzle electrode is used instead, the range of permitted voltages for the formation of the cone-jet is usually very small. This wide range of voltage differences have been covered by the different levels of the nozzle and ring voltage applied in this study.

It is noteworthy that ring voltage has more obvious effect on collection efficiency which is also declared by Taguchi results shown in Table 6. This is because the polarized ring electrode stabilizes the EHDA spray and it could be better controlled by reducing the radial electric field component on the jet.[39] The stability of the jet spraying to produce particles produced on the collecting plate would be more dependent on the ring voltage than nozzle voltage for the range of electrical potential difference tested in this study. Figure 6 shows that the differences between collection efficiencies for different nozzle voltages are not substantial; however, this is more significant for ring voltage. This figure also confirms that for each setting of nozzle and ring voltage, the collection efficiency decreases with increasing solution flow rate.

The most important feature in determining the electric fields in the EHDA process would be the voltage difference between the ring and nozzle.[40] Ding et al. (2005), reported that as the voltage difference between the ring and nozzle decreases, the spray mode could change from a multiple cone spray to a single spray cone, then finally to a dripping model The dripping mode appears when the voltage difference is small and this can cause a significant reduction in collection efficiency as spraying of particles would be disrupted. In fact, the polymer and drug solution would be lost in drippings instead of being atomized.

In other words, the difference between nozzle and ring voltages has a more significant effect on both particle size[18–21,40] and collection efficiency. The effect of voltage difference between nozzle and ring is illustrated in Figure 7. This figure shows that higher collection efficiency occurs at higher voltage difference between nozzle and ring. In addition to the formation of the stable cone-jet at high voltage differences between the nozzle and ring, this phenomenon may be related to the size of the fabricated particles. Xie et al. (2007), reported that particle size decreases with increasing voltage difference between nozzle and ring. As mentioned, the smaller size of the particles causes electrical field force to be predominant. Therefore, increasing voltage difference between nozzle and ring can produce smaller particles and higher particle collection efficiency.

Effect of Electrical Conductivity and Polymer Material. The low electrical conductivity of DCM (0.0023 μS/cm) is another factor in the dripping of solution that lowers the collection efficiency. As the electrical conductivity of DCM is just above the threshold value to get a cone-jet, the small electrical conductivity affects the induction of electric stresses to overcome the surface tension of the liquid. Figure 8 shows the variation of particle collection efficiency versus electrical conductivity of the solution for two different polymers, PLGA and PLA. It can be observed in this figure that with increasing

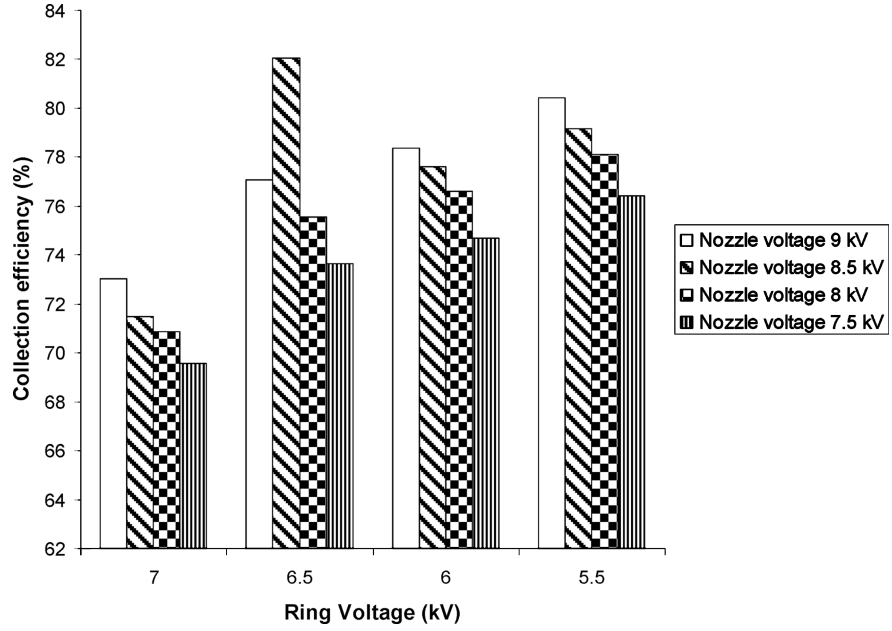

Figure 7. Variation of collection efficiency for four example ring voltage settings versus nozzle voltages.

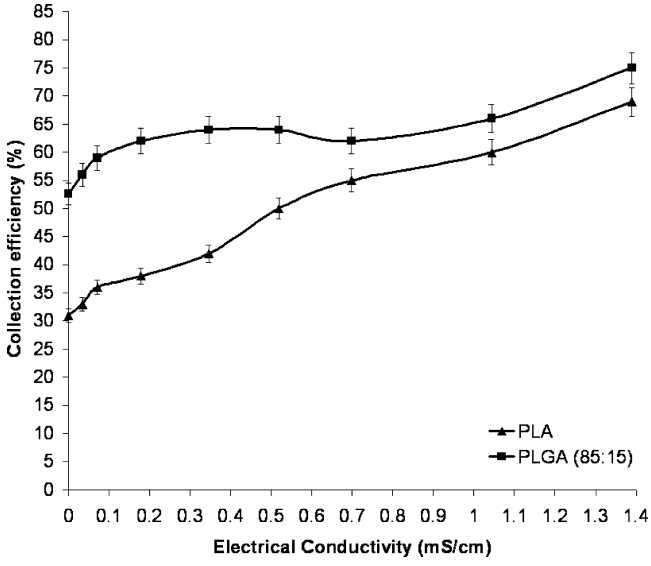

Figure 8. Variation of particle collection efficiency versus electrical conductivity of the solution for two different polymers, PLGA and PLA, at 8.5 kV nozzle voltage, 7 kV ring voltage, 2 mL/h solution flow rate, and 25 L/min nitrogen flow rate.

electrical conductivity of the solution, the collection efficiency increases. With increasing conductivity, a better distribution of charges can be reached on surface of the cone at the tip of the nozzle. This improved distribution of charge results in a more stable cone jet which obtains a higher collection efficiency. Furthermore, the variation in solution flow conductivity results in a drastic change in the final particle size based on the following equation.[41]

$$d \propto \left(\frac{1}{K}\right)^{1/6} \tag{11}$$

Equation 11 shows that increases in solution conductivity causes the particle size to be decreased. It was discussed that decreases in particle size can result in increasing particle collection efficiency. It can be observed in Figure 8 that the collection efficiency of solution prepared by PLA is smaller. The molecular weight of PLGA (85:15) is much smaller than the molecular weight of PLA. The high molecular weight of PLA can drastically affect the cone formation process. It was observed that the solution preparation with PLA took much longer than preparation with PLGA. This observation indicates that the viscosity of the solution prepared by PLA is higher. An overly high viscosity of the sprayed solution prevented stable cone-jet mode and production of mondisperse droplets. High viscosity of PLA solution also caused partial clogging of the capillary, thus resulting in deviance in spraying direction. Due to the high concentration and high molecular weight of PLA, ultrathin film and even tapered particles emerge from the collection plate. Therefore, the particle collection efficiency will be decreased.

Other Possible Factors. Four factors mentioned in the previous sections were identified and their effects on collection efficiency were investigated using the Taguchi method. Apart from these four factors, there may be other minor factors affecting the collection efficiency that were not tested. One of these factors could be the accumulation of the particles on the collecting plate throughout the encapsulation process. Although this has aided in the evaporation of DCM on the particles,

Table 7. Summary of Factors, Levels, Obtained Results (Particle Size) and *S/N* Ratio in Each Trial

trial no.	nozzle voltage (kV)	ring voltage (kV)	soln. flow rate (mL/h)	nitrogen flow rate (L/min)	particle size 1 (μm)	particle size 2 (μm)	*S/N*
1	9	7	2.5	35	9.1	9.2	19.228
2	9	6.5	2	30	8.9	8.9	18.987
3	9	6	1.5	25	8.1	8.3	18.274
4	9	5.5	1	20	6.7	6.6	16.455
5	8.5	7	2	25	8.7	9	18.935
6	8.5	6.5	2.5	20	7.9	7.9	17.952
7	8.5	6	1	35	7.3	7.1	17.144
8	8.5	5.5	1.5	30	7.8	7.9	17.896
9	8	7	1.5	20	9	9	19.084
10	8	6.5	1	25	8.3	8.7	18.581
11	8	6	2.5	30	9.8	9.9	19.868
12	8	5.5	2	35	9.2	9.2	19.275
13	7.5	7	1	30	7.6	7.5	17.558
14	7.5	6.5	1.5	35	7.8	7.5	17.668
15	7.5	6	2	20	10	10.1	20.043
16	7.5	5.5	2.5	25	10.2	10.2	20.172

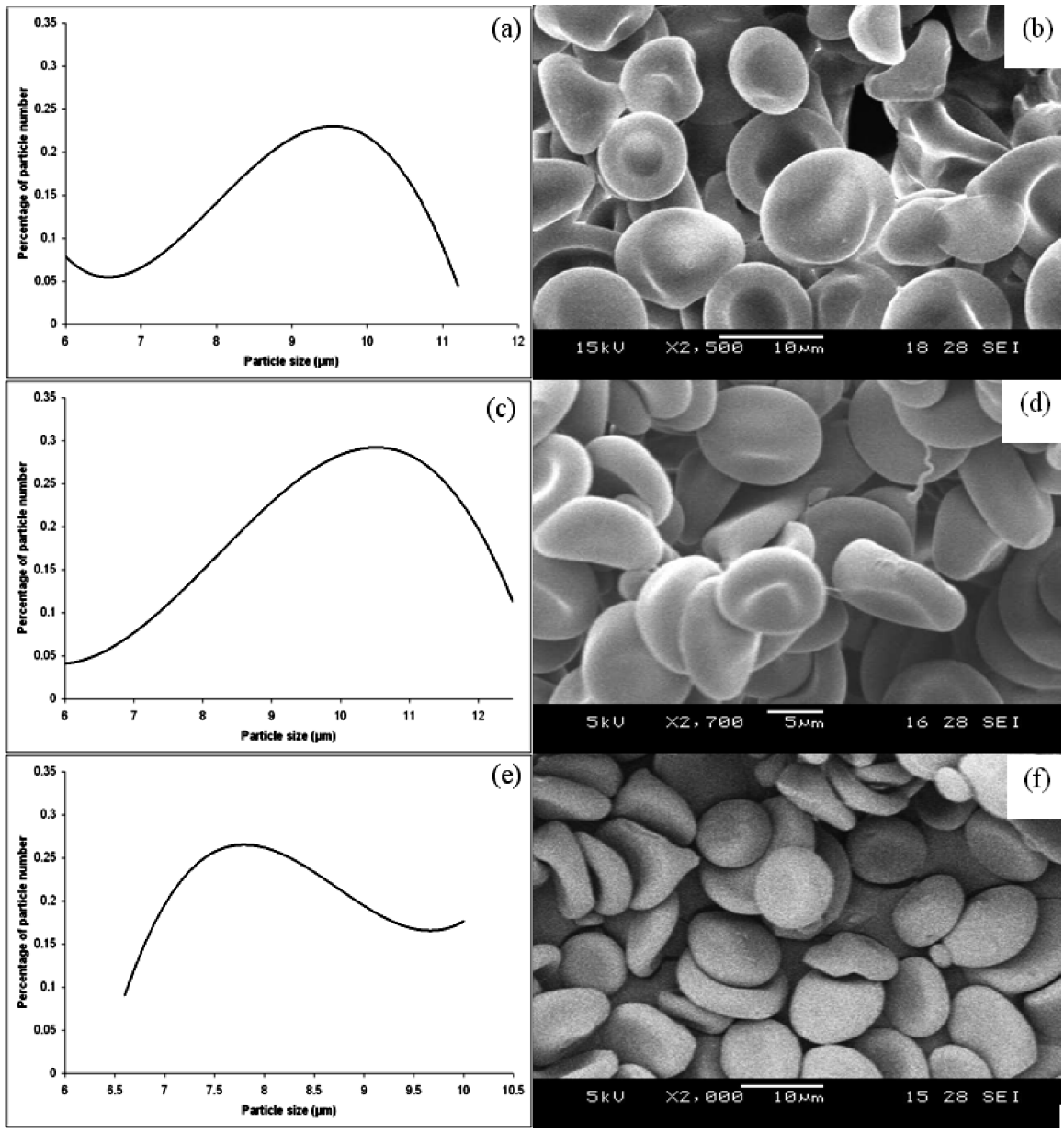

Figure 9. Particle size distribution and related SEM photo for the following conditions: Nozzle voltage 8.5 kV, Ring voltage 7 kV, solution flow rate 2 mL/h and nitrogen flow rate 25 L/min (a) and (b), Nozzle voltage 7.5 kV, Ring voltage 6 kV, solution flow rate 2 mL/h and nitrogen flow rate 20 L/min (c) and (d), Nozzle voltage 8.5 kV, Ring voltage 5.5 kV, solution flow rate 1.5 mL/h and nitrogen flow rate 30 L/min (e) and (f).

electrical charges can build up on the collecting plate and this can affect electric field inside the chamber[42] and subsequently affect the EHDA process. This factor may also affect the production rate and collection efficiency of the particles on the collecting plate. It was previously mentioned that the distance from the nozzle tip to the collecting plate is long and the exposure of air can actually discharge the particles. However, since the particles are agglomerated on the collecting plate and this process may induce the recharging of the particles.

Particle Size Analysis. The particle size measurement for each trial can be observed in Table 7. Particle size distributions for some of the trials are shown in Figure 9. The results of the Analysis of Variance (ANOVA) can also be observed in Table 8. The *F*-ratio for ring voltage and nitrogen flow rate shown in Table 8 is equal to zero and thus the effect may be regarded as insignificant and neglected. Table 8 shows that solution flow rate is a more important factor than nozzle voltage for determining the particle size. In Table 8, the calculated error is about 39% which is less than the limit. It means that almost all effective factors have been considered and the error of the experiment is not significant.

It was found that particle size can be fine-tuned with variation of solution flow rate. Figure 10 shows the variation of arithmetic particle mean size versus solution flow rate for different nozzle voltages. In the cone-jet model, the following scaling law can be used to describe the relationship between droplet size and various process variables:[3,36]

$$I \propto (\gamma K Q)^{1/2} \tag{12}$$

$$d = c\left(\frac{\rho_l \varepsilon_0 Q^4}{I^2}\right)^{1/6} \propto Q^{1/2} \tag{13}$$

These equations indicate that the droplet size can decrease with decreasing solution flow rate. On the basis of Figure 10, the sizes of fabricated particles were found to decrease with decreasing solution flow rate. Since the droplet size has a direct relation with the particle size at a fixed polymer concentration,

Table 8. Results of Analysis of Variance (ANOVA) in Particle Size Measurements for Each Factor

	factors	DOF[a]	sum of squares	variance	*F*-ratio	pure sum	percent
1	nozzle voltage	3	3.765	1.255	2.247	2.090	12.159
2	ring voltage	3	0.699	0.233	0.417	0.000	0.000
3	solution flow rate	3	9.968	3.322	5.950	8.293	48.252
4	nitrogen flow rate	3	1.078	0.359	0.644	0.000	0.000
5	error/others	3	1.674	0.558			39.589
6	total	15	17.187				100.0

[a] Degree of freedom.

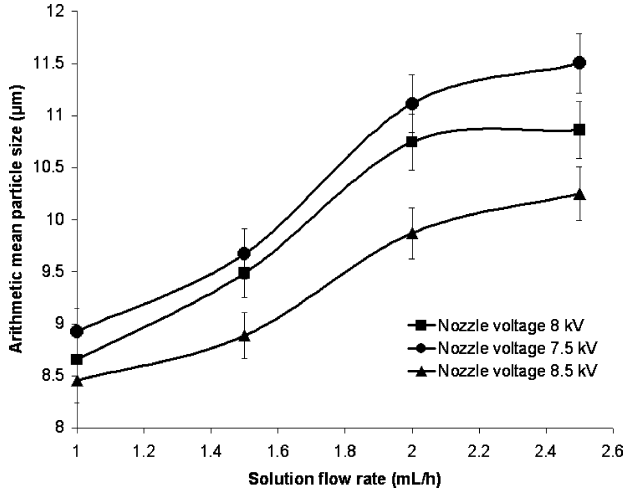

Figure 10. Variation of arithmetic particle mean size versus solution flow rate for different nozzle voltages at ring voltage 6 kV and nitrogen flow rate 25 L/min.

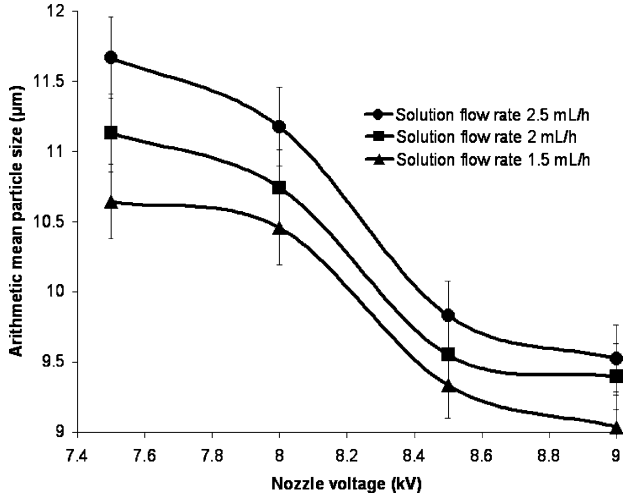

Figure 11. Variation of arithmetic particle mean size versus nozzle voltage for different solution flow rates at ring voltage 6 kV and nitrogen flow rate 25 L/min.

our experimental results are quantitatively consistent with the prediction by eq 13. Figure 10 also confirms that in a fixed solution flow rate and ring voltage, increasing nozzle voltage decreases the particle size which can be further explained in Figure 11 below.

Ding et al. (2005) stated that at a fixed solution flow rate and system geometry, the voltage difference between nozzle and ring plays a key role in determining the spray pattern. Figure 11 shows the variation of arithmetic mean particle size versus nozzle voltage at different solution flow rates. The ring voltage is fixed in this figure; therefore, an increase in nozzle voltage can result in an increasing voltage difference between nozzle and ring. Voltage difference between nozzle and ring has a direct relation with the electrical field strength. Since the electrical polarization forces exerts in the opposite direction of surface tension forces, the electrical field can suppress the surface tension. Xie et al. (2007) reported that with increase in nozzle voltage, dripping frequency could increase and the size of the droplet could decrease. The radius of atomized droplet under the voltage difference V is given by the following:[43]

Table 9. Summary of Factors, Levels, Obtained Results (Concentration of DCM) and *S/N* Ratio in Each Trial

trial no.	nozzle voltage (kV)	ring voltage (kV)	soln. flow rate (mL/h)	nitrogen flow rate (L/min)	concentration of DCM 1 (ppm)	concentration of DCM 2 (ppm)
1	9	7	2.5	35	154.87	47.63
2	9	6.5	2	30	226.97	90.34
3	9	6	1.5	25	56.02	51.42
4	9	5.5	1	20	48.46	92.89
5	8.5	7	2	25	271.6	107.52
6	8.5	6.5	2.5	20	298.42	178.55
7	8.5	6	1	35	147.99	150.61
8	8.5	5.5	1.5	30	68.14	61.57
9	8	7	1.5	20	19.71	60.7
10	8	6.5	1	25	88.93	65.97
11	8	6	2.5	30	250.43	150
12	8	5.5	2	35	281.68	145.55
13	7.5	7	1	30	272.5	48.05
14	7.5	6.5	1.5	35	242.43	136.26
15	7.5	6	2	20	300.95	194.73
16	7.5	5.5	2.5	25	84.71	142.97

$$R_d = \sqrt[3]{\frac{3}{2\rho_l g}\left[r_0\gamma - 2\varepsilon_0\left(\frac{V^2}{\ln\left(\frac{4H}{r_0}\right)}\right)\right]} \qquad (14)$$

On the basis of eq 14, an increase in nozzle voltage (at a fixed ring voltage) can result in decrease in droplet size, which has a direct relation with particle size. Figure 11 confirms that the experimental results are consistent with the prediction by eq 14.

Concentration of Residual DCM in Particles. Using the integration equation resulted from GC/MS experiment, the concentration of DCM could be found for all the trials as listed in Table 9. Since each trial was repeated in duplicate, two concentrations of DCM can be seen in this table. As shown in this table, the residual DCM content of the particles fabricated using the EHDA method was below the safety standards margin (600 ppm)[25] at the end of the process. This is achieved even without using freeze-drying process which is used to evaporate the residual solvent in the fabricated particles.

The low concentration of residual DCM on the particles could be achieved without freeze-drying because of the following reasons. First, the distance from the nozzle tip to the edge of collecting plate is longer than the corresponding distance in the previous prototype of the chamber. Because of this longer distance, the droplets from the cone-jet at the nozzle tip can have more time to travel through the electric field to the collecting plate. Therefore, the residual organic solvents in the droplets have more time to evaporate. Second, the collecting plate is designed in such a way that the particles stay on the collecting plate throughout the EHDA process. The particles deposit on the collecting plate in the cross-flow of flow of nitrogen in the encapsulation chamber. Consequently, the organic solvent on the particles would evaporate easily due to the prolonged exposure to the nitrogen cross-flow.

It is predicted that the residual amount of organic solvent in the particles would depend on the nitrogen flow rate in the

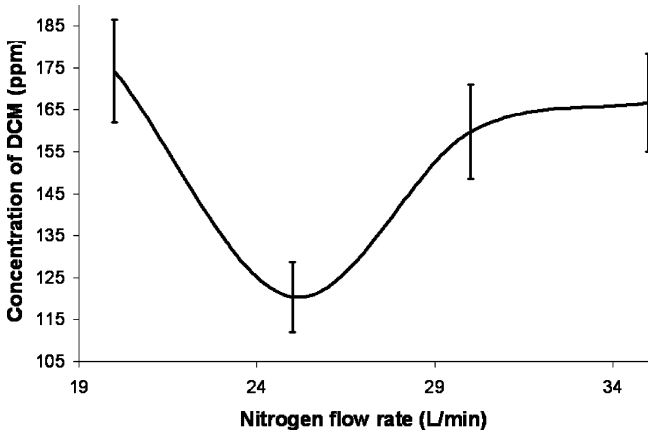

Figure 12. Variation of residual concentration of DCM in collected particles versus nitrogen flow rate.

encapsulation process and would be independent of other factors. Different values of DCM concentration for the same nitrogen flow rates in the trials mentioned in Table 9 can probably be related to the different durations of time in the encapsulation process for the different trials. Figure 12 shows that the concentration of DCM in particles decreases with increasing nitrogen flow rate from 20 to 25 L/min, but it increases with increasing nitrogen flow rate from 25 to 35 L/min and approaches to a constant value for higher nitrogen flow rates.

An increase in nitrogen flow rate from 20 to 25 mL/min improves the convective mass transfer around the particles and expedites the evaporation of DCM from the particles without affecting the flight time of the particles in the encapsulation chamber. In contrast, the convective mass transfer around the particles is also improved with increasing nitrogen flow rates from 25 to 35 L/min but the flight time of the particles is shortened and this results in the increase in the DCM concentration in particles.

Conclusions

A new generation of shuttle glass chamber was used in this study to fabricate biodegradable polymeric microparticles for drug delivery applications. This new shuttle glass chamber, in contrast to the previous prototypes, had a cylindrical shape with larger diameter of nitrogen inlet and outlet in which particles were collected inside the chamber. The effect of solution flow rate, nitrogen flow rate, nozzle, and ring voltage on the particle collection efficiency and residual amount of organic solvent in collected particles were investigated. The experimental study was designed and analyzed by the Taguchi statistical method. The results shown in Table 5 verified that most effective factors had been considered. The Taguchi analysis showed that the most important factor affecting particle collection efficiency was the solution flow rate. Moreover, on the basis of the quantitative analysis, ANOVA, nitrogen flow rate and ring voltage appeared to contribute the most to the results. An F-ratio less than 1 showed that the effect of the nozzle voltage could be regarded as insignificant and the important factors were listed in the following order: solution flow rate, nitrogen flow rate, and ring voltage. ANOVA was also used to estimate the collection efficiency at the optimum condition of 1 mL/h solution, 35 L/min nitrogen, and 6 kV ring voltage. The calculated collection efficiency, 82.04% was, within the range of the confidence limit of the measured value, 79.4%.

In addition to the quantified factors mentioned before, duration of the encapsulation process was considered as a minor adjustable factor which can also affect the electrical field in the chamber and therefore can influence the particle collection efficiency. Another factor, electrical conductivity of solution, can also affect the cone-jet mode and thus affecting the particle collection efficiency. Higher electrical conductivity of solution results in more stable cone jet and higher collection efficiency. Moreover, high molecular weight polymers like PLA cause instability in cone jet and therefore reducing the collection efficiency.

The size of fabricated particles was drastically affected by solution flow rate and nozzle voltage. Increasing nozzle voltage (at fixed ring voltage) and decreasing solution flow rate can result in the reduction of the particle size.

Residual solvent in collected particles was another issue perused in this study. Gas chromatography/mass spectrometry (GC/MS) was used to determine the residual content of DCM in the collected particles. For all of the trials, the residual DCM content of the particles fabricated using the EHDA method was well within the safety standards (<600 ppm) at the end of process without applying freeze-drying which is usually used after EHDA process. The long distance from the spray zone to the collecting plate is the main reason for achieving the low concentration of residual DCM in the collected particles. Furthermore, the design of the system for allowing particles to reach the collecting plate for a long exposure time throughout the encapsulation chamber is another reason for achieving a low quantity of residual DCM in the collected particles. The findings of the present work clearly show that high collection efficiency and low concentration of residual solvent in collected particles can be achieved with good adjustment on the operating parameter of the EHDA encapsulation chamber.

Nomenclature

u = particle velocity vector, m s^{-1}
m_p = mass of the particle, kg
F_q = columbic repulsion force, kg m s^{-2}
F_E = electrical field force, kg m s^{-2}
F_B = buoyancy force, kg m s^{-2}
F_g = gravitational force, kg m s^{-2}
F_D = drag force, kg m s^{-2}
C_D = drag coefficient
R_p = particle radius, m
d = particle diameter, m
n = number of particles
u_v = inert gas velocity, m s^{-1}
ρ_p = particle density, kg m^{-3}
ρ_f = fluid (inert gas) density, kg m^{-3}
g = gravitational acceleration, m s^{-2}
E = electrical field vector, V m^{-1}
q = particle charge, C
r_i = distance between the particle of concern and surrounding particles, m
r_i = unit vector showing the direction of the exerted repulsive force between the particles
K = electrical conductivity, S m^{-1}
I = current, C/s
γ = liquid surface tension, N/m
ρ_l = liquid density, kg m^{-3}
Q = solution flow rate, m^3 s^{-1}
c = a constant
R_d = droplet radius, m
r_0 = radius of nozzle, m
H = distance between the tip of the nozzle and collecting plate, m

Acknowledgment

This work is supported by the National University of Singapore under Grant No. R279-000-222-112.

Literature Cited

(1) Almekinders, J. C.; Jones, C. Multiple jet electrohydrodynamic spraying and applications. *J. Aerosol Sci.* **1999**, *30*, 969–971.

(2) Tatemoto, Y.; Ishikawa, R.; Takeuchi, M.; Takeshita, T.; Noda, K.; Okazaki, T. An electrospray methos using a multi-capillary nozzle emitter. *Chem. Eng. Technol.* **2007**, *30*, 1274–1279.

(3) Hartman, R. P. A.; Brunner, D. J.; Camelot, D. M. A.; Marijnissen, J. C. M.; Scarlett, B. Electrohydrodynamic atomization in the cone-jet mode; physical moeling of the liquid cone and jet. *J. Aerosol Sci.* **1999**, *30*, 823–849.

(4) Hayati, I.; Bailey, A. I.; Tadros, TH F. Investigations into the mechanisms of electrohydrodynamic spraying of liquids: 1. Effect of electric field and the environment on pendant drops and factors affecting the formation of stable jets and atomization. *J. Colloids Interf. Sci.* **1987**, *117*, 205–221.

(5) Barrero, A.; Ganan-Calvo, A. M.; Fernandez-Feria, R. The role of liquid viscosity and electrical conductivity on the motions inside Taylor cones in E.H.D. spraying of liquids. *J. Aerosol Sci.* **1996**, *27*, 175–176.

(6) Farook, U.; Zhang, H. B.; Edirisinghe, M. J.; Stride, E.; Saffari, N. Preparation of microbubble suspensions by co-axial electrohydrodynamic atomization. *Med. Eng. Phys.* **2007**, *29*, 749–754.

(7) Lopez-Herrera, J. M.; Ganan-Calvo, A. M.; Perez-Saborid, M. One dimensional simulation of the breakup of capillary jets of conducting liquids; application to E.H.D. spraying. *J. Aerosol Sci.* **1999**, *30*, 895–912.

(8) Lastow, O.; Balachandran, W. Novel low voltage EHD spray nozzle for atomization of water in the cone jet mode. *J. Electrostatics* **2007**, *65*, 490–499.

(9) Noymer, P. D.; Garel, M. Stability and atomization characteristics of electrohydrodynamic jets in the cone-jet and multi-jet modes. *J. Aerosol Sci.* **2000**, *31*, 1165–1172.

(10) Ragucci, R.; Fabiani, F.; Cavaliere, A.; Muscetta, P.; Noviello, C. Characterization of stability regimes of electrohydrodynamically enhanced atomization. *Exp. Therm. Fluid Sci.* **2000**, *21*, 156–161.

(11) Lenggoro, I. W.; Widiyandari, H.; Hogan Jr., C. J.; Biswas, P.; Okuyama, K. Colloidal nanoparticle analysis by nanoelectrospray size spectrometry with a heated flow. *Anal. Chim. Acta* **2007**, *585*, 193–201.

(12) Ku, B. K.; Kim, S. S. Electrohydrodynamic spraying characteristics of glycerol solutions in vacuum. *J. Electrostatic* **2003**, *57*, 109–128.

(13) Christopher, J.; Hogan, Jr.; Yun, K. M.; Chen, D. R.; Lenggoro, I. W.; Biswas, P.; Okuyama, K. Controlled size polymer particle production via electrohydrodynamic atomization. *Colloids Surf., A* **2007**, *311*, 67–76.

(14) Wenlei, J.; Gupta, R. K.; Deshpande, M. C.; Schwendeman, S. P. Biodegradable poly(lactic-co-glycolic acid) microparticles for injectable delivery of vaccine antigens. *Adv. Drug Delivery Rev.* **2005**, *57*, 391–410.

(15) Kreuter, J. Nanoparticulate systems for brain delivery of drugs. *Adv. Drug Delivery Rev.* **2001**, *47*, 65–81.

(16) Ciach, T. Microencapsulation of drugs by electro-hydro-dynamic atomization. *Int. J. Pharm.* **2006**, *324*, 51–55.

(17) Hong, Y.; Li, Y.; Yin, Y.; Li, D.; Zou, G. Electrohydrodynamic atomization of quasi-monodisperse drug-loaded spherical/wrinkled microparticles. *J. Aerosol Sci.* **2008**, *39*, 525–536.

(18) Xie, J.; Marijnissen, J. C. M.; Wang, C. H. Microparticles developed by electrohydrodynamic atomization for the local delivery of anticancer drug to treat C6 glioma in vitro. *Biomaterials* **2006**, *27*, 3321–3332.

(19) Xie, J.; Wang, C. H. Electrospray in the dripping mode for cell microencapsulation. *J. Colloids Interf. Sci.* **2007**, *312*, 247–255.

(20) Yao, J.; Lim, L. K.; Xie, J.; Hua, J.; Wang, C. H. Characterization of electrospraying process for polymeric particle fabrication. *J. Aerosol Sci.* **2008**, *39*, 987–1002.

(21) Huang, Z. M.; Zhang, Y. Z.; Kotaki, M.; Ramakrishna, S. A review on polymer nanofibers by electrospinning and their applications in nanocomposites. *Compos. Sci. Technol.* **2003**, *63*, 2223–2253.

(22) Meng, F.; Jiang, Y.; Sun, Z.; Yin, Y.; Li, Y. Electrohydrodynamic liquid atomization of biodegradable polymer microparticles: effect of electrohydrodynamic liquid atomization variables on microparticles. *J. Appl. Polym. Sci.* **2009**, *113*, 526–534.

(23) Ijsebaert, J. C.; Geerse, K. B.; Marijnissen, J. C. M.; Lammers, J. W. J.; Zanen, P. Electro-hydrodynamic atomization of drug solutions for inhalation purposes. *J. Appl. Physiol.* **2001**, *91*, 2735–2741.

(24) Rhodes, M. *Introduction to Particle Technology*; John Wiley & Sons: West Sussex, 2008.

(25) Hemin, N.; Wang, C. H. Fabrication and characterization of PLGA/HAp composite scaffolds for delivery of BMP-2 plasmid DNA. *J. Controlled Release* **2007**, *120*, 111–121.

(26) Park, S. K.; Kim, K. D.; Kim, H. T. Preparation of silica nanoparticles: Determination of the optimal synthesis conditions for small and uniform particles. *Colloids Surf., A* **2002**, *197*, 7–17.

(27) Idris, A.; Ismail, A. F.; Noordin, M. Y.; Shilton, S. J. Optimization of cellulose acetate hollow fiber reverse osmosis membrane production using Taguchi method. *J. Membr. Sci.* **2002**, *205*, 223–237.

(28) Rezvanpour, A.; Roostaazad, R.; Hesampour, M.; Nystrom, M.; Ghotbi, C. Effective factors in the treatment of kerosene-water emulsion by using UF membranes. *J. Hazardous Mat.* **2009**, *161*, 1216–1224.

(29) Allen, T. *Powder Sampling and Particle Size Determination*; Elsevier: USA, 2003.

(30) Chein, R.; Chung, J. N. Particle dynamics in a gas-particle flow over normal and inclined plates. *Chem. Eng. Sci.* **1998**, *43*, 1621–1636.

(31) Crowe, C. T.; Troutt, T. R.; Chung, J. N.; Davis, R. W.; Moore, E. F. A Turbulent Flow without Particle Mixing. *Aerosol Sci. Technol.* **1995**, *22*, 135–138.

(32) Huang, Y.; Wu, W.; Zhang, H. Numerical study of particle dispersion in the wake of gas-particle flows past a circular cylinder using discrete vortex method. *Powder Tech.* **2006**, *162*, 73–81.

(33) Yang, Y.; Chung, J. N.; Troutt, T. R.; Crowe, C. T. The effects of particles on the stability of a two-phase wake flow. *Int. J. Multiphase Flow* **1993**, *19*, 137–149.

(34) Taguchi, G. *System of Experimental Design. Engineering Methods to optimize quality and minimize costs*; White Plains: New York, 1987.

(35) Grace, J. M.; Marijnissen, J. C. M. A review of liquid atomization by electrical means. *J. Aerosol Sci.* **1994**, *25*, 1005–1019.

(36) Hartman, R. P. A.; Brunner, D. J.; Camelot, D. M. A.; Marijnissen, J. C. M.; Scarlett, B. Jet break-up in electrohydrodynamic atomization in the cone-jet mode. *J. Aerosol Sci.* **2000**, *31*, 65–95.

(37) Cloupeau, M.; Prunet-Foch, B. Electrohydrodynamic spraying functioning modes: a critical review. *J. Aerosol Sci.* **1994**, *25*, 1021–1036.

(38) Lindblad, N. R.; Schneider, J. M. Production of uniform-sized liquid droplets. *J. Sci. Instrum.* **1965**, *42*, 635–638.

(39) Borra, J. P.; Hartmann, R.; Marijnissen, J.; Scarlett, B. Destabilisation of sprays in the cone-jet mode by electrical discharges on the jet. *J. Aerosol Sci.* **1996**, *27*, 203–204.

(40) Ding, L.; Lee, T.; Wang, C. H. Fabrication of monodispersed Taxol-loaded particles using electrohydrodynamic atomization. *J. Controlled Release* **2005**, *102*, 395–413.

(41) Xie, J.; Lim, L. K.; Phua, Y.; Hua, J.; Wang, C. H. Electrohydrodynamic atomization for biodegradable polymeric particle production. *J. Colloids Interf. Sci.* **2006**, *302*, 103–112.

(42) Ciach, T. Application of Electro-hydro-dynamic Atomization in Drug Delivery. *J. Drug Deliv. Sci. Tech.* **2007**, *17*, 367–375.

(43) Burgarski, B.; Amsden, B.; Neufeld, R. J.; Poncelet, D.; Goosen, M. F. A. Effect of electrode geometry and charge on the production of polymer microbeads by electrostatics. *Can. J. Chem. Eng.* **1994**, *72*, 517–521.

Received for review January 25, 2010
Revised manuscript received September 30, 2010
Accepted October 25, 2010

IE1009662